Mon. Not. R. Astron. Soc. **326,** 1134–1140 (2001)

The long-period orbit of the dwarf nova V630 Cassiopeiae

Jerome A. Orosz,[1★†] John R. Thorstensen[2] and R. Kent Honeycutt[3]

[1]*Astronomical Institute, Utrecht University, 3508 TA Utrecht, the Netherlands*
[2]*Department of Physics and Astronomy, 6127 Wilder Laboratory, Dartmouth College, Hanover, NH 03755, USA*
[3]*Astronomy Department, Indiana University, Bloomington, IN 47405, USA*

Accepted 2001 May 11. Received 2001 April 2

ABSTRACT

We present extensive spectroscopy and photometry of the dwarf nova V630 Cassiopeiae. A late-type (K4–5) absorption spectrum is easily detectable, from which we derive the orbital parameters. We find a spectroscopic period of $P = 2.56387 \pm 4 \times 10^{-5}$ d and a semi-amplitude of $K_2 = 132.9 \pm 4.0\,\mathrm{km\,s^{-1}}$. The resulting mass function, which is a firm lower limit on the mass of the white dwarf, is then $f(M) = 0.624 \pm 0.056\,\mathrm{M_\odot}$. The secondary star is a 'stripped giant' and, using relations between the core mass and the luminosity and between the core mass and the radius, we derive a lower limit of $M_2 \geqslant 0.165\,\mathrm{M_\odot}$ for the secondary star. The rotational velocity of the secondary star is not resolved in our spectra and we place a limit of $V_{\rm rot} \sin i < 40\,\mathrm{km\,s^{-1}}$. The long-term light curve shows variations of up to 0.4 mag on short (1–5 d) time-scales, and variations of 0.2–0.4 mag on longer (3–9 months) time-scales. In spite of these variations, the ellipsoidal light curve of the secondary star is easily seen when the data are folded on the spectroscopic ephemeris. Ellipsoidal models fitted to the mean light curve give an inclination in the range $66\overset{\circ}{.}96 \leqslant i \leqslant 78\overset{\circ}{.}08$ (90 per cent confidence). This inclination range, and the requirement that $M_2 \geqslant 0.165\,\mathrm{M_\odot}$ and $V_{\rm rot} \sin i < 40\,\mathrm{km\,s^{-1}}$, yields a white dwarf mass of $M_1 = 0.977^{+0.168}_{-0.098}\,\mathrm{M_\odot}$ and a secondary star mass of $M_2 = 0.172^{+0.029}_{-0.012}\,\mathrm{M_\odot}$ (90 per cent confidence limits). Our findings confirm the suggestion of Warner that V630 Cas is a rare example of a dwarf nova with a long orbital period.

Key words: techniques: photometric – techniques: spectroscopic – binaries: close – stars: dwarf novae – stars: individual: V630 Cas – novae, cataclysmic variables.

1 INTRODUCTION

V630 Cassiopeiae (V630 Cas) is a poorly studied cataclysmic variable star. This star had a 4.8-mag outburst in 1950 (Whitney 1973), and a 2-mag outburst observed in late 1992 (Honeycutt et al. 1993). The optical spectrum in quiescence shows absorption lines indicative of a late K star and low-level excitation emission lines (Szkody & Howell 1992). V630 Cas is classified in the Duerbeck (1987) catalogue as a likely WZ Sagittae-type dwarf nova, a particular subtype of outbursting cataclysmic variable star that has relatively large-amplitude outbursts and relatively long intervals between outbursts. However, based on its similarity to BV Cen, GK Per and V1017 Sgr, Warner (1994) suggested that V630 Cas is a rare example of a dwarf nova with a long orbital period. Warner (1994) predicted a period of ≈6 d, based on a correlation between the orbital period and the recurrence time between outbursts, and on a correlation between the orbital period and the rate of rise to outburst. We have collected spectroscopic observations of the source over a number of years, and from these we show that the orbital period is indeed relatively long with $P = 2.56387 \pm 0.00004$ d. We also present a long-term *V*-band light curve of the source. Our observations allow us to derive reasonably precise component masses and other interesting binary parameters. We discuss our observations and analysis, and the implications of these below.

2 OBSERVATIONS

2.1 Photometry

This V630 Cas photometry was obtained by RoboScope (Honeycutt & Turner 1992), an unattended 0.41-m telescope in central Indiana that is devoted to long-term photometric monitoring of accretion systems. The data were reduced using the method of incomplete ensemble photometry (Honeycutt 1992). The ensemble solution used 76 comparison stars and 579 charge-coupled device (CCD) exposures obtained over the interval 1991

★ Visiting Astronomer at Kitt Peak National Observatory, which is operated by the Association of Universities for Research in Astronomy Inc., under a cooperative agreement with the National Science Foundation.
†E-mail: J.A.Orosz@astro.uu.nl

July to 2000 November; the zero-point was established using 12 secondary standards from Henden & Honeycutt (1995). Fig. 1 shows the complete light curve, including an extended 3-month long outburst in 1992. This 2-mag outburst was described in Honeycutt et al. (1993), and further discussed in Warner (1994). We also see in Fig. 1 a rise of ∼0.2 mag over the four years following the outburst. This is followed by a similar ∼0.2 mag decline during the succeeding four years. Superimposed on this 1993–96 rise and 1997–2000 decline is an additional ∼0.2 mag of scatter that substantially exceeds the observational error. There are changes of up to 0.4 mag that are unresolved at our typical data spacing of 1 to 5 d, superimposed on resolved 0.2–0.4 mag changes with time-scales of 3 to 9 months.

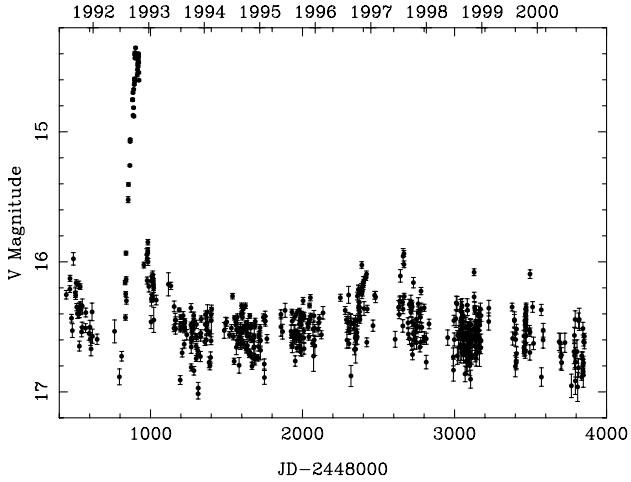

Figure 1. The RoboScope *V*-band light curve of V630 Cas, complete until 2000 November.

Table 1. Journal of spectroscopy.

Date (UT)	*N*	UT start	UT end	Telescope
1993-12-08	2	6:49	7:03	KPNO 4 m
1993-12-10	18	1:21	7:17	KPNO 4 m
1994-11-05	6	2:53	3:50	KPNO 4 m
1994-11-06	11	1:47	9:24	KPNO 4 m
1994-11-07	11	1:44	3:50	KPNO 4 m
1995-10-01	3	2:51	4:35	WIYN 3.5 m
1995-10-02	2	4:58	5:22	WIYN 3.5 m
1995-10-03	2	2:56	3:33	WIYN 3.5 m
1997-09-19	2	5:41	10:46	MDM 2.4 m
1997-09-20	2	4:37	11:54	MDM 2.4 m
1997-09-21	1	9:19	–	MDM 2.4 m
1997-09-22	1	8:55	–	MDM 2.4 m
1997-09-23	2	2:37	9:20	MDM 2.4 m
1998-01-28	1	4:13	–	MDM 2.4 m
1998-01-31	1	2:25	–	MDM 2.4 m
1998-02-03	1	3:05	–	MDM 2.4 m
1999-06-13	1	10:43	–	MDM 2.4 m
1999-10-19	1	9:24	–	MDM 2.4 m
1999-10-21	1	9:46	–	MDM 2.4 m
1999-10-22	1	9:01	–	MDM 2.4 m
1999-11-06	1	1:55	–	WHT 4.2 m
1999-12-21	1	20:10	–	WHT 4.2 m
2000-01-06	1	3:17	–	MDM 2.4 m
2000-01-07	1	4:34	–	MDM 2.4 m
2000-01-08	1	4:51	–	MDM 2.4 m

N is the number of velocities included in the analysis; for the MDM data, each velocity represents the sum of several exposures, typically of 8 min duration. Times given are heliocentric times of mid-exposure of the first and last velocity each night.

2.2 Spectroscopy

Table 1 is a journal of the spectroscopic observations. The Kitt Peak National Observatory (KPNO) 4-m spectra were taken with the R/C spectrograph and a CCD detector, and covered λλ4450–6930 with ∼3 Å resolution; individual exposures were typically 600 s. At the MDM Hiltner 2.4-m telescope we used the modular spectrograph and a grating covering 4300–7400 Å with 3 Å resolution, but with considerable vignetting towards the ends. The WIYN spectra were from the Hydra multifibre instrument; these had inferior signal-to-noise ratio and resolution, but proved useful in confirming the ephemeris (below). The spectra from the 4.2-m William Hershel Telescope (WHT) were obtained through the service programme of the Isaac Newton Group of telescopes on La Palma. The instrumental configuration consisted of the red arm of ISIS and the R1200R grating, yielding ≈1 Å resolution near Hα. The two spectra each consist of the median of three consecutive 20-min exposures. We were careful to maintain an accurate wavelength calibration for all the observations. We reduced the raw CCD pictures to one-dimensional, wavelength-binned, flux-calibrated spectra using standard techniques implemented in IRAF.[1]

3 ANALYSIS

3.1 Spectroscopic period

Our spectra of V630 Cas show Balmer emission lines, emission lines of helium (most notably the lines at λλ5876 and 6678) and relatively strong absorption lines from an ≈K-type star (see Fig. 2). Similar features were also noted by Szkody & Howell (1992). To measure the absorption spectrum radial velocities, we obtained spectra of K-type stars using the same equipment, and cross-correlated these with the V630 Cas spectra using the IRAF tasks FXCOR (Tonry & Davis 1979) and XCSAO (Kurtz & Mink 1998). The cross-correlations mostly yielded formal error estimates $<10\,\mathrm{km\,s^{-1}}$, but the mutual agreement of the standard stars suggests that systematic effects limited the uncertainty of a single velocity to $\sim15\,\mathrm{km\,s^{-1}}$.

We searched for periods in the absorption velocities by fitting them with sinusoids over a sufficiently dense grid of test frequencies, from 0.01 to over 4 cycle $\mathrm{d^{-1}}$. Fig. 3 shows the result, plotted as the inverse of the mean square residual of the fit. This period-finding method should be especially suitable for the present data, in which the periodic signal is expected to be accurately sinusoidal and the modulation is expected greatly to exceed the noise. In this circumstance a very large spike is expected at the correct frequency, because the small scatter at that frequency results in a much tighter fit than at incorrect frequencies. This expectation is borne out here – a frequency near 0.39 cycle $\mathrm{d^{-1}}$

[1] IRAF is distributed by the National Optical Astronomy Observatories, which are operated by the Association of Universities for Research in Astronomy Inc., under cooperative agreement with the National Science Foundation.

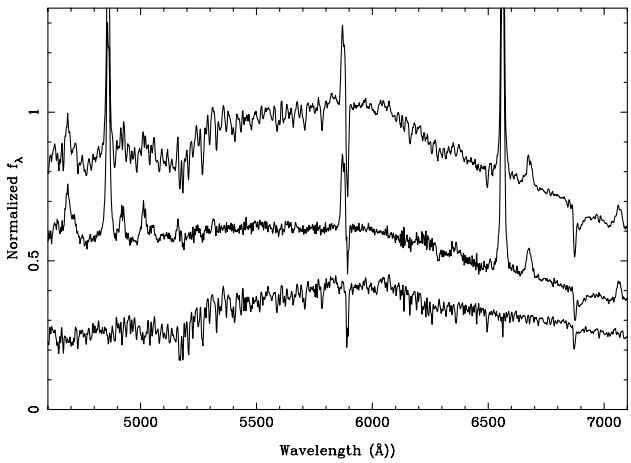

Figure 2. Top: The averaged spectrum (in the rest frame of the secondary) from the 1994 KPNO observations, normalized to unity at 5500 Å. Bottom: The spectrum of HD 333388 (a K5 dwarf) observed with the same instrumentation. The spectrum was normalized to unity at 5500 Å and scaled by 0.38. Middle: The difference spectrum, which is essentially the spectrum of the accretion disc.

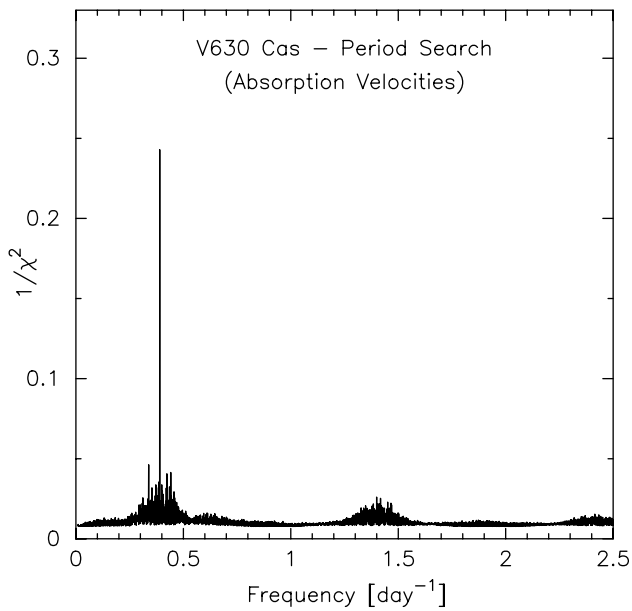

Figure 3. The results of the period search on the absorption line velocities.

stands out prominently, reflecting a uniquely good fit near 2.56 d. The single sharp spike shows that the cycle count is uniquely determined over the 6-yr span of the observations. Table 2 gives parameters of the best sinusoidal fit to the observations, and the folded radial velocity curve is shown in Fig. 4.

The emission lines were generally single-peaked, with the exception of the spectra from 1994 November 7, which had double-peaked profiles with an average peak-to-peak separation of $410 \pm 35\,\mathrm{km\,s^{-1}}$. We measured the radial velocities of the Hα emission lines using the double-Gaussian technique of Shafter (1983). The Gaussians had a full width at half-maximum of 8 Å and the separation between them was 24 Å. The emission-line radial velocities are shown folded on the orbital period in Fig. 4. There is a great deal of scatter, but the emission-line radial velocities are generally out of phase with respect to the absorption-line radial velocities. The formal semi-amplitude of the emission-line radial

Table 2. Spectroscopic elements.

Parameter	Value
Period, absorption lines (d)	$2.563\,87 \pm 4 \times 10^{-5}$
K_2 velocity, absorption lines ($\mathrm{km\,s^{-1}}$)	132.9 ± 4.0
γ_2 velocity, absorption lines ($\mathrm{km\,s^{-1}}$)	-87.3 ± 2.3
T_0, absorption lines (HJD 240 0000+)	$4\,9994.4340 \pm 0.0087$
Period, emission lines (d)	$2.563\,75 \pm 1.2 \times 10^{-4}$
K_1 velocity, emission lines ($\mathrm{km\,s^{-1}}$)	39.1 ± 4.9
γ_1 velocity, emission lines ($\mathrm{km\,s^{-1}}$)	-111.4 ± 2.7
T_0, emission lines (HJD 240 0000+)	$4\,9662.566 \pm 0.034$

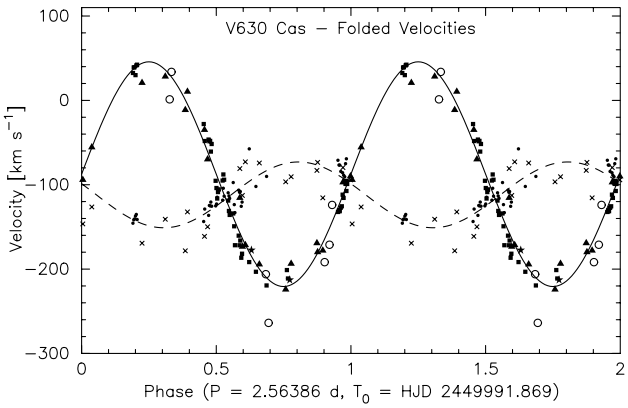

Figure 4. The phased absorption-line and emission-line velocities and the corresponding best-fitting sinusoids. The plot symbols are: filled squares, KPNO 4-m absorption line; open circles, WIYN Hydra absorption line; filled triangles, MDM 2.4-m absorption line; five-pointed star, WHT absorption line; small round dots, KPNO 4-m Hα emission velocities; and small crosses, MDM Hα emission velocities.

velocity curve is $K_1 = 39\,\mathrm{km\,s^{-1}}$. However, we would not rely on the emission-line radial velocity curve to derive any dynamical information given the large scatter seen in the velocities.

3.2 Phase-averaged light curve

We have folded the post-outburst data on the spectroscopic ephemeris. Before performing this folding, the post-outburst data for each year were normalized to a magnitude of 16.5 to remove the long multiyear trend seen in the post-outburst data of Fig. 1. This decreases the scatter in the folded light curve but does not correct for the 3–9 month changes seen in Fig. 1. Fig. 5 shows this folded light curve with superposed averages over phase bins 0.05 phase units wide. We also constructed a binned light curve by computing the median V magnitude within each of 20 phase bins using the unnormalized light curve (excluding the outburst). The resulting binned light curve is statistically identical to the binned light curve shown in Fig. 5. Thus we are reasonably confident that the binned light curve shown in Fig. 5 represents the true long-term averaged light curve.

3.3 Spectral type of the secondary

We used the technique outlined in Marsh, Robinson & Wood (1994) to find the best-fitting spectral type of the secondary star and to derive the spectrum of the accretion disc. For this we used 26 flux-calibrated spectra from 1994 November, observed with the KPNO 4-m telescope. Each spectrum was Doppler-shifted to zero

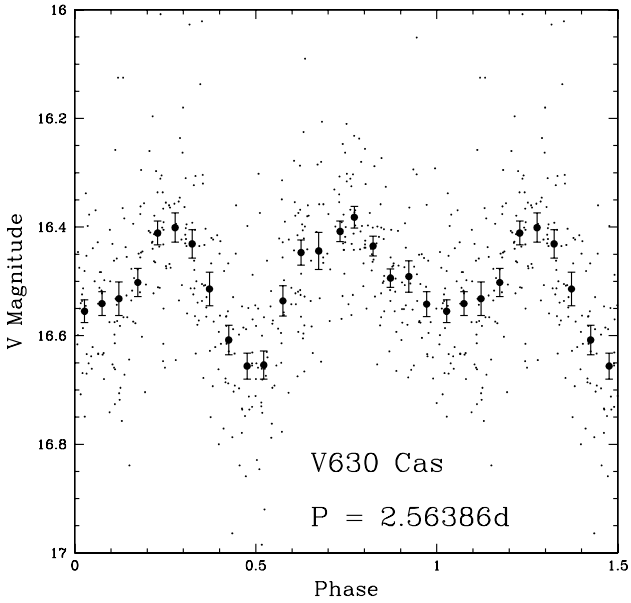

Figure 5. The folded post-outburst *V*-band light curve (small dots). The large filled circles are averages over phase bins 0.05 phase units wide.

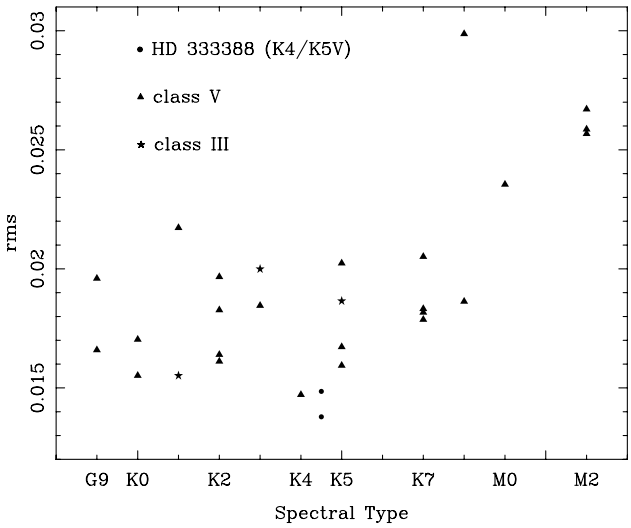

Figure 6. The rms versus spectral type for the 31 template spectra (see text). The two lowest rms values, and hence the best spectral type match, are for the two observations of HD 333388, a K4–5 dwarf (filled circles). The stars are the three luminosity class III templates, and the triangles are the luminosity class V templates.

velocity (using the spectroscopic elements in Table 2) before the averaged spectrum was made. This averaged spectrum, shown as the top spectrum in Fig. 2, has a signal-to-noise ratio of ≈100 over much of the wavelength range. We have 31 observations of 21 different stars (mostly dwarfs) observed with the KPNO 4-m (13 spectra were from 1993 and 18 spectra were from 1994). The rest-frame spectrum and the template spectra were all normalized to unity at 5500 Å. Then each template was scaled by a weight factor w, and subtracted from the rest-frame spectrum. The scatter in the difference spectrum is measured by computing the rms from a fourth-order polynomial fit to the 676 points in the wavelength intervals 5200–5800 Å and 5950–6500 Å. The template spectrum that gives the lowest overall rms, corresponding to the smoothest difference spectrum, is deemed to be the best match for the spectrum of the secondary star.

The secondary must be evolved well off the main sequence owing to the long orbital period. We have only three luminosity class III templates (the rest are luminosity class V). However, our experience with this decomposition technique indicates that it is not sensitive to the luminosity class of the template at these low resolutions. Fig. 6 shows the rms values as a function of the spectral type for all of the templates. The best two matches were provided by two different observations of HD 333388, which are classified in the SIMBAD database as K8V. However, we believe HD 333388 has been misclassified. We adopt K4–5V based on a comparison with our other templates, most notably spectra of 61 Cyg A (a K5V standard) and 61 Cyg B (a K7V standard). Apart from HD 333388, the rms values tend to be the lowest near K4 and K5. The K7 and later templates clearly give worse fits, and the templates earlier than K2 also give relatively poor fits, although the difference is not as dramatic as for the later templates. We adopt K4–5 for the spectral type of the secondary in V630 Cas.

Fig. 2 shows the results of the decomposition. The top spectrum is the observed normalized rest-frame spectrum. The bottom spectrum is the normalized spectrum of HD 333388, scaled by 0.38. The spectrum in the middle is the difference between the two. The stellar absorption lines are removed reasonably well, and the only remaining features are the emission lines, the interstellar Na D line and the atmospheric feature near 6870 Å. The emission lines near 4921 and 5015 Å seen in the difference spectrum are probably due to He I. The weak emission line near 5169 Å might be part of the Fe II multiplet 42 (the other two lines would be at 4924 and 5018 Å, Moore 1972).

We repeated this general procedure using the higher-resolution spectra in an attempt to measure the rotational velocity of the secondary star. In this case we have only one template spectrum, that of HD 3765, a K2V star. The template spectrum was broadened by various trial values of $V_{\rm rot}\sin i$ using the standard analytic rotational broadening kernel (e.g. Gray 1992) with a linear limb-darkening coefficient of 0.6 and compared to the spectrum of V630 Cas. The rotational broadening is not resolved, and we place an upper limit of $V_{\rm rot}\sin i < 40\,{\rm km\,s^{-1}}$.

3.4 Light-curve models

The binned light curve shown in Fig. 5 has the characteristics of the well-known ellipsoidal variations, namely two maxima of roughly equal height per orbital cycle and two minima of unequal depth per orbital cycle. The character of the ellipsoidal variations is a strong function of the inclination i and the mass ratio Q. Therefore, in principle, one can determine the orbital inclination and mass ratio by modelling the light curve. In practice, however, there are difficulties, which can introduce systematic errors into the ellipsoidal modelling. In the case of V630 Cas, the light from the accretion disc dilutes the observed ellipsoidal modulations of the secondary star. The primary minimum in the light-averaged light curve is relatively deep (it is more than 0.1 mag deeper than the secondary minimum); this larger-than-expected depth is almost certainly due to a grazing eclipse of the star by the disc. There is also a great deal of variability that is not associated with the ellipsoidal modulations. However, with the large number of observations the short-term excursions all seem to 'average out', and we are reasonably confident that the mean light curve represents the true ellipsoidal light curve (which is of course diluted by the disc).

We used the ELC code (Orosz & Hauschildt 2000) to model the

binned light curve. We use specific intensities from the NEXTGEN models (Hauschildt, Allard & Baron 1999a; Hauschildt et al. 1999b). The ELC code can include light from a flared accretion disc, and geometrical effects due to the disc (i.e. eclipses of the secondary star) are accounted for. We have the usual geometrical parameters for the ellipsoidal model, namely the inclination i, the mass ratio Q and the orbital separation a. The main parameters for the secondary star are its filling factor f, its rotational velocity with respect to synchronous Ω, its gravity darkening exponent β, its albedo A and its mean (or effective) temperature $T_{\rm eff}$. We assume the star is exactly Roche lobe filling and rotating synchronously, hence $f = 1$ and $\Omega = 1$. We set $\beta = 0.08$ and $A = 0.5$, the usual values for a star with a convective outer envelope. Finally, the spectral type of the secondary star in V630 Cas is K4–5. The temperature corresponding to this depends on the gravity. For example, a K4V star ($\log g = 4.60$) nominally has a temperature of 4791 K, whereas a K4III star ($\log g = 1.7$) nominally has a temperature of 4113 K, according to the parameters given in Gray (1992). A simple two-dimensional interpolation gives $T_{\rm eff} = 4310$ K for a K4.5 star with $\log g = 3$ (see below). The parameters

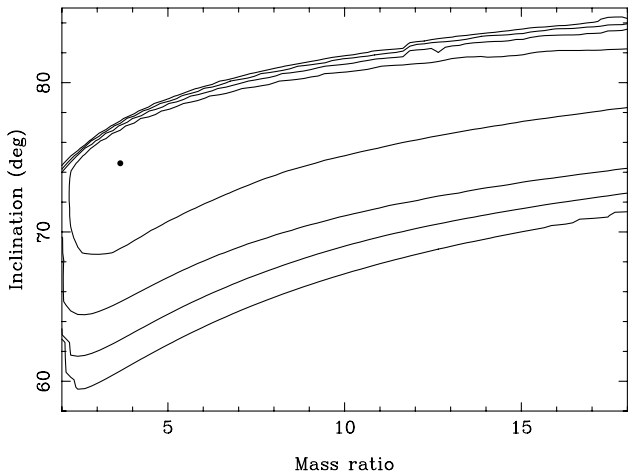

Figure 7. Contours of χ^2 values in the mass ratio–inclination plane from the light-curve fitting. The filled circle marks the location of the minimum χ^2 value. The contours shown correspond to the 68.3, 95.4, 99.73 and 99.99 per cent confidence levels for two parameters of interest.

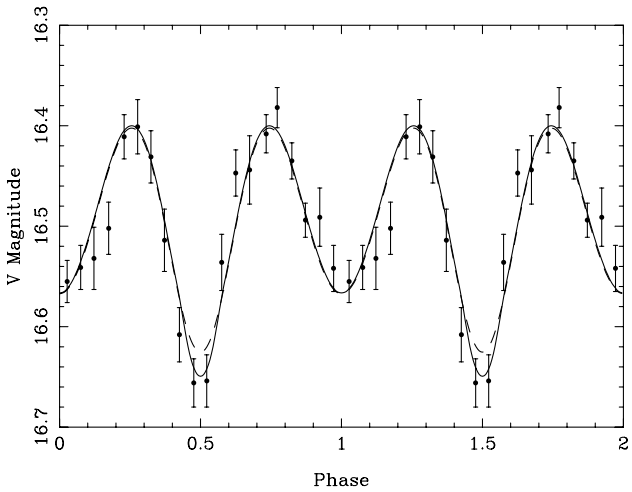

Figure 8. The phase-averaged V-band light curve and the ellipsoidal model (solid line). The dashed line is a model with light from the disc but no eclipses.

describing the disc are its inner radius $R_{\rm inner}$, its outer radius $R_{\rm outer}$, the flaring angle of the rim $\beta_{\rm rim}$, the temperature of the inner edge $T_{\rm disc}$ and the power-law exponent of the disc temperature profile ξ, where $T(r) = T_{\rm disc}(r/r_{\rm inner})^{\xi}$. Unfortunately, the disc parameters are not that well constrained, for a number of reasons. For example, we have light curves in only one band, so the general slope of the disc spectral energy distribution is relatively unconstrained. In addition, the bright central parts of the disc are not eclipsed, so it is more difficult to pin down the disc brightness profile. We therefore fixed the inner and outer radii, the flaring angle and the power-law exponent at reasonable values ($R_{\rm inner} \approx 0.01\,{\rm R}_{\odot}$, $R_{\rm outer} = 75$ per cent of the primary Roche radius $R_{\rm RL}$, $\beta_{\rm rim} = 2°$, and $\xi = -0.4$, a value that gives a flatter profile than the nominal value of $\xi = -3/4$ expected for a steady-state disc). The only remaining free parameter for the disc is then the temperature at its inner edge $T_{\rm disc}$. Values of $T_{\rm disc}$ near 9000 K give an integrated V-band intensity roughly equal to the integrated V-band intensity of the star, which is consistent with the observations (e.g. the spectral decomposition shown in Fig. 2). One should bear in mind that the source shows considerable variability about its mean, hence the 'disc fraction' measured in Fig. 2 may be slightly larger or smaller than the true long-term average. Finally, although the ELC code can include the white dwarf, we omitted the white dwarf for simplicity. Since the white dwarf is not eclipsed, its only contribution to the light curve would be constant in phase. Hence there is no real constraint on its temperature and brightness. Since we have only observations in one bandpass, we can alter slightly the inner radius and inner temperature of the disc to mimic the contribution from the white dwarf.

We are left with basically four free parameters: the inclination i, the mass ratio Q, the orbital separation a and the temperature of the inner edge of the disc $T_{\rm disc}$. The two binary observables we have are the radial velocity curve of the secondary star and the V-band light curve. To carry out the fitting of the observables, we defined a grid of points in the Q–i plane with steps in Q of 0.1 and steps in i of 0.°25. At each Q,i point in the grid, a and $T_{\rm disc}$ are optimized using a 'grid search' routine adapted from Bevington (1969) so that the total χ^2 is minimized:

$$\chi^2_{\rm total} = \chi^2_V + \chi^2_{RV} = \sum_{i=1}^{20} \frac{(V_{\rm obs} - V_{\rm mod})_i^2}{\sigma_i^2} + \sum_{i=1}^{60} \frac{(RV_{\rm obs} - RV_{\rm mod})_i^2}{\sigma_i^2}. \quad (1)$$

The errors on the radial velocities were scaled to yield $\chi^2_{RV}/\nu = 1$ for the best-fitting sinusoid. Fig. 7 shows the contour plot of $\chi^2_{\rm total}$ in the Q–i plane. The inclination is fairly well constrained to be near 75°, whereas the mass ratio Q is basically not constrained (we can put independent constraints on the mass ratio, see Section 4.2). There is a dramatic and abrupt increase in the χ^2 values near 80°. At this and higher inclinations substantial eclipses are predicted, and since none are observed the quality of the fits rapidly gets worse. At inclinations smaller than about 60° the amplitude of the model is far too small to match the observations, and the quality of the fits also gets much worse. The only observational constraint we have from the spectra is that roughly half of the light is not from the secondary star. Our models generally satisfy this constraint.

Fig. 8 shows the V light curve and the adopted model (solid line) with $Q = 5.5$ and $i = 74°$ (see Section 4.2). The fit is good ($\chi^2 = 21.39$ for 20 points). There is a grazing eclipse of the star by the outer edge of the disc. The dashed line in Fig. 8 shows what the light curve would look like if this eclipse is not accounted for

(the constant light from the disc is still included). The general fitting results are not too sensitive to the assumed disc radius. We know the disc contributes about half of the light, and if a large part of the disc is eclipsed then we would expect an ≈0.7 mag deep eclipse at phase 0. We do not observe such an eclipse, which means that the bright central parts of the disc are not eclipsed. This in turn constrains the inclination to be less than about 80°. In the same vein, the overall amplitude of the light curve is relatively large (≈0.25 mag) *in the presence of substantial disc light*. Thus the inclination cannot be too small. For most mass ratios, inclinations smaller than about 65° produce models with amplitudes that are too small to match the observations.

4 ASTROPHYSICAL CONSEQUENCES

Having laid out all of the observation of V630 Cas, we now discuss some of the astrophysical implications of these observations.

4.1 Mass limits on the components

The observed radial velocity curve of the secondary star K_2 can be used to place a straightforward lower limit on the mass of the unseen accreting star M_1:

$$M_1 > f(M) \equiv \frac{PK_2^3}{2\pi G} = \frac{M_1 \sin^3 i}{(M_1 + M_2)^2} = 0.624 \pm 0.056\,\mathrm{M}_\odot, \qquad (2)$$

where M_2 is the mass of the secondary star and G is the universal constant of gravitation.

If the secondary star is near the giant branch in the Hertzsprung–Russell (HR) diagram, we can estimate the mass of its core (and therefore a lower limit on the secondary star M_2) using three basic relations obtained on the evolutionary models of 'stripped giants'. The luminosity and radius of the core are strong functions of the core mass $M_{\rm core}$ (e.g. Taam 1983; Webbink, Rappaport & Savonije 1983; also Phinney & Kulkarni 1994):

$$\frac{L_{\rm core}}{\mathrm{L}_\odot} = \left(\frac{M_{\rm core}}{0.16\,\mathrm{M}_\odot}\right)^8, \qquad (3)$$

$$\frac{R_{\rm core}}{\mathrm{R}_\odot} = 1.3\left(\frac{M_{\rm core}}{0.16\,\mathrm{M}_\odot}\right)^5. \qquad (4)$$

We also have, from Roche geometry and Kepler's third law, a relationship between the mean density of the Roche lobe filling secondary star and the orbital period:

$$\rho = \frac{M_2}{\frac{4}{3}\pi R_2^3} = \frac{3\pi}{P^2 G R_{\rm RL}^3(Q)}\frac{1}{1+Q}, \qquad (5)$$

where $Q = M_1/M_2$ and $R_{\rm RL}(Q)$ is the sphere-equivalent radius of the Roche lobe for unit separation. For $2 \leqslant Q \leqslant 20$, the quantity $R_{\rm RL}^{-3}(Q)(1+Q)^{-1}$ is approximately constant (it varies between 9.7 and 10.16). Thus, for our case here, the mean density of the secondary star is a function only of the orbital period to a good approximation. Therefore the Roche radius is a function only of the mass of the secondary star. The procedure for finding $M_{\rm core}$ is simple. For an *assumed* core mass $M_{\rm core}$ we know its radius $R_{\rm core}$ and luminosity $L_{\rm core}$ (equations 3 and 4). For an *assumed* envelope mass $M_{\rm env}$ we know the total mass of the secondary M_2 and hence its radius R_2 using equation (5). The radius of the secondary star and the luminosity $L_{\rm core}$ can then be used to find the effective temperature $T_{\rm eff}$. Fig. 9 shows a contour plot of $T_{\rm eff}$ in the $M_{\rm core}$–$M_{\rm env}$ plane for situations where $R_{\rm core} < R_2$. The contour lines are nearly vertical, meaning that the core mass $M_{\rm core}$ is tightly constrained whereas the envelope mass $M_{\rm env}$ is not. According to Fig. 9, $T_{\rm eff} = 4300$ K corresponds to $M_{\rm core} \geqslant 0.165\,\mathrm{M}_\odot$. Hence the lower limit on the secondary star mass is $M_2 \geqslant 0.165\,\mathrm{M}_\odot$.

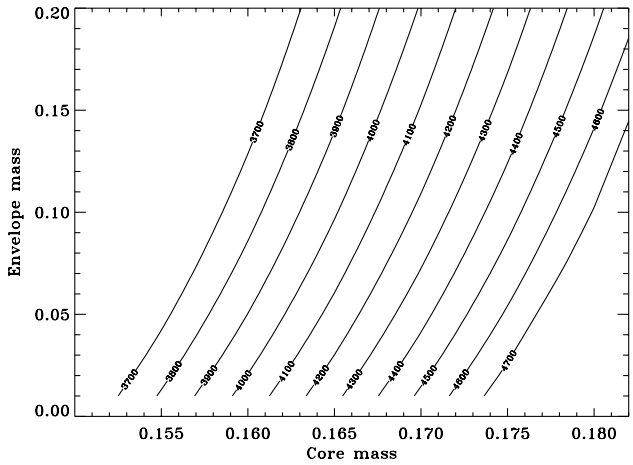

Figure 9. Contours of the effective temperature $T_{\rm eff}$ in the core mass–envelope mass plane computed using the relations in Section 4.1.

4.2 Binary parameters

We use a Monte Carlo procedure outlined in Orosz & Wade (1999) to derive interesting binary parameters and their uncertainties from the results of the light-curve fitting. Since we have the radial velocity curve of the secondary star, each point in the mass ratio–inclination plane corresponds uniquely to a set of binary parameters (e.g. component masses, orbital separation, etc.). Each point in the mass ratio–inclination plane also has a certain probability based on the χ^2 value of the light-curve fit. The Monte Carlo procedure selects parameter sets equally from different probability intervals and generates probability distributions for each binary parameter of interest. Since we do not know the mass function (equation 2) of the accreting star exactly, 20 values of $f(M)$ are drawn randomly from the appropriate Gaussian distribution at each Q–i point in the plane. We have three additional constraints that we add to the Monte Carlo procedure. The first constraint, $M_1 > f(M) = 0.624\,\mathrm{M}_\odot$, is automatically satisfied. The second constraint is the one derived from the stripped giant evolution, namely $M_2 > 0.165\,\mathrm{M}_\odot$. The third constraint is the upper limit on the rotational velocity, $V_{\rm rot} \sin i < 40\,\mathrm{km\,s^{-1}}$. For a Roche lobe filling star in synchronous rotation,

$$\frac{V_{\rm rot}\sin i}{K_2} = \frac{R_{\rm RL}(Q)}{a}\left(\frac{1+Q}{Q}\right). \qquad (6)$$

The upper limit of $V_{\rm rot}\sin i < 40$ implies $Q > 5$ for $K_2 = 132.9\,\mathrm{km\,s^{-1}}$. The results of the Monte Carlo procedure are shown in Table 3.

The mass of the white dwarf is quite close to $1\,\mathrm{M}_\odot$, while the mass of the secondary star is only slightly above the lower limit imposed by the core mass: the hydrogen envelope has a mass of only $\approx 0.01\,\mathrm{M}_\odot$. The predicted rotational velocity of the secondary star ($38\,\mathrm{km\,s^{-1}}$) is just below our upper limit of $40\,\mathrm{km\,s^{-1}}$. As expected from the relatively long orbital period, the orbital separation and secondary star radius are relatively large for a cataclysmic variable ($8.3\,\mathrm{R}_\odot$ and $2\,\mathrm{R}_\odot$, respectively). The small

Table 3. Astrophysical parameters for V630 Cas.

Parameter	Central value	90 per cent ranges
i (deg)	74.007	66.962–78.083
Mass ratio	5.476	4.959–6.105
M_1 ($M_\odot$)	0.976	0.880–1.141
M_2 ($M_\odot$)	0.172	0.165–0.197
Total mass ($M_\odot$)	1.170	1.039–1.325
Orbital separation ($R_\odot$)	8.269	8.024–8.687
R_2 ($R_\odot$)	2.014	1.965–2.110
L_2 (bolometric, $L_\odot$)	1.285	1.001–1.839
log g_2 (cgs units)	3.071	3.058–3.090
$V_{\rm rot} \sin i$ (km s^{-1})	38.464	37.257–40.000

Additional constraints are $M_2 > 0.165\,M_\odot$ and $V_{\rm rot} \sin i < 40\,{\rm km\,s^{-1}}$. The quoted uncertainties are at 90 per cent confidence.

mass and large radius of the secondary combine to give a surface gravity of $\log g = 3.07$, considerably smaller than the gravities of late-type main-sequence K stars ($\log g = 4.6$, Gray 1992).

5 DISCUSSION

The orbital period of 2.56 d is relatively long for a cataclysmic variable (CV). The Ritter & Kolb (1998) catalogue shows only two CVs with longer periods. V1017 Sgr is a dwarf nova with a period of 5.714 d (Sekiguchi 1992), and MR Vel is a supersoft X-ray source with an orbital period of 3.832 903 d (Schmidtke et al. 2000). Two other long-period CVs are GK Per, with a period of 1.996 803 d (Crampton, Cowley & Fisher 1986), and the old nova X Ser, with a period of 1.478 d (Thorstensen & Taylor 2000). Based on the similarity between V630 Cas, GK Per, V1017 Sgr and also BV Cen, Warner (1994) speculated that V630 Cas is a rare example of a long-period dwarf nova. Based on correlations between the orbital period P and recurrence time T and rate of rise τ,

$$\log T \approx -0.1 + 1.7 \log P, \tag{7}$$

$$\log \tau \approx 0.95 + 0.7 \log P, \tag{8}$$

where P is in days, T is in years and τ is in days per magnitude, Warner (1994) predicted an orbital period of $\approx$6 d for V630 Cas, more than twice the actual value. A period of 2.56 d implies $\tau = 17.2\,{\rm d\,mag^{-1}}$ and $T = 3.9$ yr. The observed rate of rise for V630 Cas is about 33 d mag^{-1}, although this is somewhat poorly defined since the two observed outbursts were not very similar. The two outbursts were separated by 42 yr, and this is much longer than the 3.9 yr derived from equation (8). Indeed, an inspection of the RoboScope light curve (Fig. 1) suggests that the recurrence time is more than 8 yr, although we cannot rule out the possibility that a short outburst occurred in a gap of the RoboScope coverage (the RoboScope light curve shown has 579 observations, with the median time between observations 1.75 d and the longest time between two observations 153 d). It seems that the correlations given by equation (8) have little predictive power at present, mainly because they are defined by very few systems at long orbital periods.

6 SUMMARY

We have presented extensive photometry and spectroscopy of the dwarf nova V630 Cas. The period is relatively long at $P = 2.56387 \pm 4 \times 10^{-5}$ d. The observed velocity of the secondary star ($K_2 = 132.9 \pm 4.0\,{\rm km\,s^{-1}}$) places a firm lower limit of $f(M) = 0.624 \pm 0.056\,M_\odot$ for the mass of the white dwarf. By modelling the ellipsoidal light curve we find an inclination between 67 and 78° (90 per cent confidence). Our upper limit on the observed rotational velocity of the secondary star of $V_{\rm rot} \sin i < 40\,{\rm km\,s^{-1}}$ implies a mass ratio greater than 5. Evolutionary considerations give a lower limit of $0.165\,M_\odot$ for the core mass of the secondary star. All of these constraints yield component masses of $M_1 = 0.977^{+0.168}_{-0.098}\,M_\odot$ for the white dwarf and $M_2 = 0.172^{+0.029}_{-0.012}\,M_\odot$ for the secondary star (90 per cent confidence limits).

ACKNOWLEDGMENTS

The work reported in this paper is based on observations collected at the William Herschel Telescope, operated on the island of La Palma by the Isaac Newton Group in the Spanish Observatorio del Roque de los Muchachos of the Instituto de Astrofisica de Canarias. It is a pleasure to thank Charles Bailyn for his assistance with the Kitt Peak National Observatory observations. JRT acknowledges support from the US National Science Foundation through grants AST-9314787 and AST-9987334. JAO was supported by a National Young Investigator award from the US National Science Foundation to Charles Bailyn. This research made use of the SIMBAD data base.

REFERENCES

Bevington P. R., 1969, Data Reduction and Error Analysis for the Physical Sciences. McGraw-Hill, New York
Crampton D., Cowley A. P., Fisher W. A., 1986, ApJ, 300, 788
Duerbeck H. W., 1987, Space Sci. Rev., 45, 1
Gray D. F., 1992, Observations and Analysis of Stellar Photospheres. Cambridge Univ. Press, Cambridge
Hauschildt P. H., Allard F., Baron E., 1999a, ApJ, 512, 337
Hauschildt P. H., Allard F., Ferguson J., Baron E., Alexander D. R., 1999b, ApJ, 525, 871
Henden A. A., Honeycutt R. K., 1995, PASP, 107, 324
Honeycutt R. K., 1992, PASP, 104, 435
Honeycutt R. K., Turner G. W., 1992, in Filipenko A., ed., Robotic Telescopes in the 1990s. Astron. Soc. Pac., San Francisco, p. 77
Honeycutt R. K., Robertson J. W., Turner G. W., Vesper D. N., 1993, PASP, 105, 919
Kurtz M. J., Mink D. J., 1998, PASP, 110, 934
Marsh T. R., Robinson E. L., Wood J. H., 1994, MNRAS, 266, 137
Moore C. E., 1972, A Multiplet Table of Astrophysical Interest. Natl. Bureau of Standards, Washington, DC, p. 66
Orosz J. A., Hauschildt P. H., 2000, A&A, 364, 265
Orosz J. A., Wade R. A., 1999, MNRAS, 310, 773
Phinney E. S., Kulkarni S., 1994, ARA&A, 32, 591
Ritter H., Kolb U., 1998, A&AS, 129, 83
Schmidtke P. C., Cowley A. P., Taylor V. A., Crampton D., Hutchings J. B., 2000, AJ, 120, 935
Sekiguchi K., 1992, Nat, 358, 563
Shafter A., 1983, ApJ, 267, 222
Szkody P., Howell S. B., 1992, ApJS, 78, 537
Taam R., 1983, ApJ, 270, 694
Thorstensen J. R., Taylor C. J., 2000, MNRAS, 312, 629
Tonry J., Davis M., 1979, AJ, 84, 1511
Warner B., 1994, Ap&SS, 222, 225
Webbink R. F., Rappaport S. A., Savonije G. J., 1983, ApJ, 270, 678
Whitney B. S., 1973, Inf. Bull. Var. Stars, No. 797

This paper has been typeset from a TEX/LATEX file prepared by the author.